Ab Initio Study of the Relative Stability and Opto-Electronics Properties of the Cu_2MgSiS_4 Compound

Saliha Ould Said[a], Kadda Amara[b,*], Belmorsli Bekki[b] and Belabbes Soudini[c]
[a]Département de Physique, Faculté Des Sciences Exactes, Université Djilali Liabés, Sidi Bel-Abbès 22000, Algeria
[b]Department of Physics, Faculty of Sciences, Dr. Tahar Moulay University of Saïda, 20000 Saïda, Algeria
[c]Applied Material Laboratory, University of Djilali Liabes, 22000 Sidi Bel Abbès, Algeria

(Received March 11, 2018)

The *ab initio* calculations based on density functional theory were performed to study structural, elastic, and opto-electronic properties of the Cu_2MgSiS_4 compound in three zinc-blende derived and one wurtzite derived structures. These calculations are carried out using the full potential linear augmented plane wave plus local orbital method, implemented into the WIEN2k computer code. Within generalized gradient approximation based on the revised Perdew–Burke–Ernzerhof exchange-correlation density functional the optimized lattice parameters and atomic positions are found to be in a good agreement with available experimental values. The total energies, obtained at equilibrium of this compound in four phases, reveal that both stannite and wurtzite-stannite are the most energetically favorable structures whereas the kesterite structure remains energetically probable under ambient conditions. The mechanical stability of this compound in these three phases is examined and established. Moreover, several isotropic elastic moduli were estimated via the calculated single crystalline elastic constants. In particular, our results show that this compound in these structures could be classified as ductile material and the highest elastic anisotropy were demonstrated by WS structure. On the other hand, the calculations of the electronic structure and optical properties were performed at the Perdew–Burke–Ernzerhof exchange-correlation density approximation level, improved by the Tran–Blaha modified Becke–Johnson potential to give an enhanced depiction of the band-gap energies and optical spectra. The fundamental band gap for the WS phase is calculated to be 2.44 eV. Analysis of the electronic structure reveals that the Cu($3d$)–S($3p$) hybridized antibonding state forms the valence band edge, while the conduction band edge is composed of the Si($3s$)–S($3p$) hybridized antibonding state. The optical response of the material in the visible and ultraviolet range is determined by calculating its complex dielectric tensor. It was observed that this compound in these three phases does not exhibit a large optical anisotropy. The estimated optical band gap 3.10 eV for WS phase is found to be in much closer agreement with the experimental findings. Over all, the obtained results seem to be more reliable compared to previous reported calculations and with available experimental results.

DOI: 10.12693/APhysPolA.135.380
PACS/topics: 71.15.Mb, 71.15.Ap, 71.20.–b, 71.22.+i

1. Introduction

The chalcogenide diamond-like semiconductors (DLSs) of quaternary type (I_2–II–IV–VI_4) have become the subject of intense research interest in recent years due to their large compositional flexibility which allows tailoring, technologically useful properties to specific needs, and make them attractive materials in the fields of tunable semiconductors [1–4], photovoltaics [1, 5, 6], spintronics [7, 8], non-linear optics [9, 10], and thermoelectrics [2, 11, 12]. These compounds can be considered as derived from either zinc-blende (ZB) or wurtzite (WZ) binary II–VI chalcogenides via the sequential cation cross-substitutions [13–15]. The derived structures, depending on their anion sublattices, can be divided in two groups, ZB derivatives and WZ derivatives. As is well known, for the DLSs compounds [16], the local charge around each anion always satisfies the octet rule in the element-substitution design of I_2–II–IV–VI_4 compounds and the mutations to the quaternary structures do not affect the tetrahedrally coordinated lattice framework of ZB or WZ. Diverse distribution schemes of the three cation species are possible leading to different space group symmetries. Among them, five main structures have been reported with the smallest primitive cells and a lower energy [14, 15], namely stannite (ST), kesterite (KS), primitive-mixed CuAu (PMCA), wurtzite-stannite (WS) and wurtzite-kesterite (WK). The variety of these materials and the number of their structures result in a richness and a considerable diversity of their properties. Much research on Cu-based quaternary chalcogenide compounds of the Cu_2–II–IV–VI_4 type has been reported [17–25], while less works on the compounds Cu_2–Mg–IV–VI_4 were undertaken.

Recently, Cu_2MgSiS_4 compound has been synthesized via high-temperature solid-state reactions and structurally characterized by single crystal X-ray diffraction analysis which reveal that this compound crystallizes in orthorhombic structure space group $Pmn2_1$ [26]. The optical absorption spectra, obtained from the optical diffuse reflectance spectra of a powder sample of this compound measured at room temperature, gives an optical band gap value of 3.20 eV. Since the band gap of this material

*corresponding author; e-mail: kamaraphy@gmail.com

exceeds the 3.1 eV, it could be interesting in the UV spectral region [27] and can be proposed as a new candidate in the high-frequency optoelectronic applications. More recently, the electronic and optical properties of $Cu_2MgSi(S_xSe_{1-x})_4$ alloys in the WS structure have been simulated [28] using the pseudo-potential plane wave (PP-PW) approach within the Heyd–Scuseria–Ernzerhof (HSE06) screened hybrid functional approximation, and for the Cu_2MgSiS_4 compound a fundamental band gap value of 3.208 eV was obtained. Our investigations are motivated by the absence or insufficiency of the reported theoretical works on the physical properties for the phases addressed herein, the WS phase belong to the orthorhombic space group $Pmn21$, the ST, KS, and PMCA phases belong to the tetragonal space groups $I\bar{4}2m$, $I\bar{4}$ and $P\bar{4}2m$, respectively.

Therefore, in this paper, we report the calculation results performed by means of the state-of-the-art *ab initio* self-consistent full potential linearised augmented plane wave plus local-orbitals (FP-LAPW+lo) method within the generalized gradient approximation based on the Perdew 2008 functional (GGA-PBEsol) [29]. Furthermore, the density of states, band structure, and optical properties have been obtained using the modified Becke–Johnson potential (TB-mBJ) [30, 31], which allows one to obtain an improved band-gap energies and optical spectra. In addition, for reliable comparison of the optical band gaps with the available theoretical and experimental values the YS-PBE0 calculations were also done for WS phase with a fixed screening parameter of $\lambda = 0.165$ bohr^{-1} which gives results close to those obtained with the HSE06 functional [32].

2. Computational details

First-principles calculations based on DFT are carried out by using the FP-LAPW+lo method as implemented in the Wien2k code [33]. In this approach, the wave function, charge density, and potential are expanded differently in two regions of the unit cell. Inside the non-overlapping spheres of the muffin-tin (MT) radius, R_{MT}, around each atom, which are taken to be 2.5, 1.80, 1.85, and 1.9 Å for Cu, Mg, Si, and S atoms, respectively, the basis set was split into core and valence subsets. The core states were treated within the spherical part of the potential only and were assumed to have a spherically symmetric charge density confined inside the MT spheres. The valence part was treated with the potential expanded in spherical harmonics to $l = 4$. The valence wave functions inside the spheres were expanded to $l = 10$ and a plane wave expansion were used in the interstitial region. To ensure convergence with minimal calculation, we tested the convergence of energy according to the k-point and the energy cut-off $R_{MT}K_{max}$. With a sufficient number of the plane wave function for $R_{MT}K_{\max} = 8$ and by using the special k-point sampling schemes which have $7 \times 7 \times 7$ grid for KS, ST, and PMCA, and $6 \times 7 \times 7$ grid for WS, 10^{-5} Ry, and 10^{-4}e as the convergence criterion for the total energy and the charge, respectively, were reached.

3. Results and discussion

3.1. Structural properties and phase stability

The crystal structures of the Cu_2MgSiS_4 compound are shown in Fig. 1. In all structures, the S atom is tetrahedrally coordinated by two Cu atoms, one Mg, and one Si atom. The Si atom is bonded to four S atoms. The KS structure is characterized by alternating cation layers of CuSi, CuMg, CuSi, and CuMg at $z = 0$, $\frac{1}{4}$, $\frac{1}{2}$ and $\frac{3}{4}$, respectively (Fig. 2c). On the other hand, in the ST structure MgSi layers alternate with Cu_2 layers (Fig. 1b). In both structures, the Si is located at the same structural site. The PMCA structure with two unit cells showed in Fig. 1d was obtained from the ST structure by interchanging the Mg and Si atoms positions in the $z = 1/2$ MgSi layer. In the WS structure, the atoms are aligned in rows when it is viewed along the z-axis, wherein each cation alternates with the sulfur anions, which form a honeycomb structure in three dimensions (Fig. 1a).

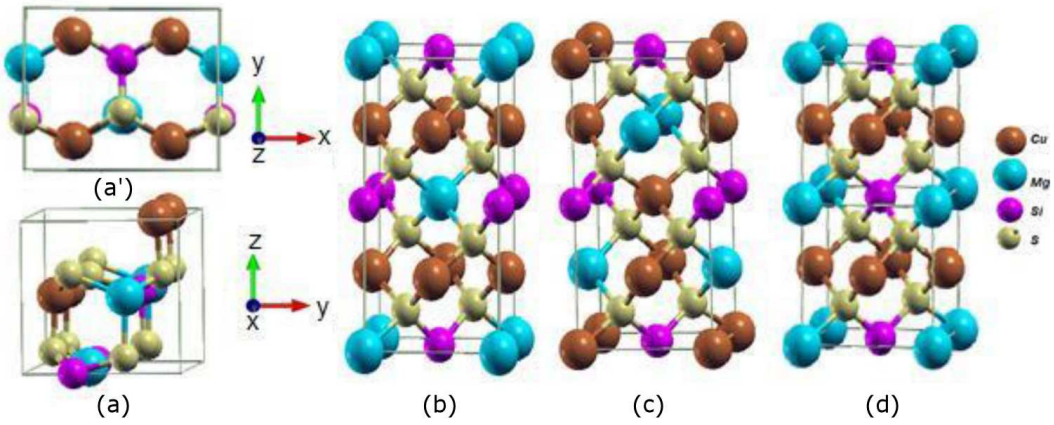

Fig. 1. The crystal structures of Cu_2MgSiS_4 in four phases (a, a') WS, (b) ST, (c) KS and (d) PMCA.

TABLE I

Equilibrium structural parameters (a [Å], b/a, c/a, equilibrium volume/f.u. (V_0 [Å^3]) and atomic positions), bulk modulus B and its pressure derivative B', the calculated difference in total energy ΔE [meV/atom] ($\Delta E = E - E_{ST}$).

Phase	a [Å]	b/a	c/a	V_0 [Å^3]	B_0 [GPa]	B'	Atomic positions					ΔE
							Atom	Site	x/a	y/b	z/c	[meV/atom]
ST	5.382	1	1.882	146.7	88.52	4.62	Cu	4d	0	0.50	0.25	0
							Mg	2a	0	0	0	
							Si	2b	0	0	0.5	
							S	8i	0.2254	0.2254	0.3717	
WS	7.524	0.845	0.816	146.8	88.09	4.62	Cu	4b	0.25223	0.17789	0.49305	0.01
	7.563[a]	0.853[a]	0.817[a]	150.7[a]					0.25258[a]	0.17753[a]	0.4935[a]	
	7.604[b]	0.848[b]	0.823[b]	153.4[b]			Mg	2a	0	0.6562	0.5033	
										0.6544[a]	0.5008[a]	
							Si	2a	0	0.3210	0.0010	
										0.3227[a]	0.0001[a]	
							S(1)	4b	0.2290	0.1587	0.1258	
									0.2286[a]	0.1643[a]	0.1210[a]	
							S(2)	2a	0	0.3010	0.6511	
										0.3083[a]	0.6574[a]	
							S(3)	2a	0	0.6447	0.1018	
										0.6368[a]	0.1078[a]	
KS	5.251	1	2.030	147.0	87.47	4.62	Cu(1)	2a	0	0	0	12.89
							Cu(2)	2c	0.50	0	0.75	
							Mg	2d	0	0.50	0.75	
							Si	2b	0.50	0.50	0	
							S	8g	0.2474	0.7245	0.1150	
PMCA	5.338	1	0.965	146.8	87.44	4.62	Cu	2f	0	0.50	0.50	29.77
							Mg	1a	0	0	0	
							Si	1d	0.50	0.5	0	
							S	4n	0.2703	0.2703	0.7480	

[a]Ref. [26] [b]Ref. [28].

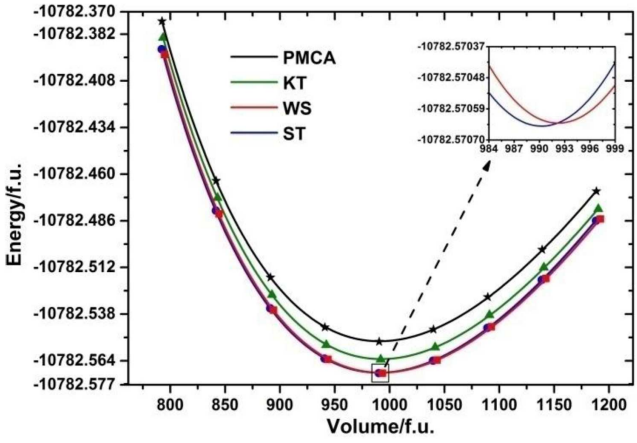

Fig. 2. Computed total energy (eV) versus unit-cell volume (Å^3) for the WS, ST, KT and PMCA structures of the Cu_2MgSiS_4 compound.

The study of relative phase stability of the system requires the knowledge of the total energies in its different structural optimized phases, or more often, the energy difference between them. Figure 2 shows the curve of total energy versus the formula unit (f.u.) volume for each phase fitted to the equation of state of Birch–Murnaghan [34, 35]. Our calculations showed that the equilibrium energies of ST and WS phases are identical; see inset in Fig. 2 and Table I. This means that the ST and WS phases can coexist or be transformed into each other. It is clearly seen that the total energy of the PMCA structure is higher than the others, which shows that it is the least stable. The calculated values of the atomic coordinates, lattice constants, equilibrium volume, bulk modulus and its pressure derivative are summarized in Table I with other available results. For the WS structure, the structural parameters are in good agreement with the experimental and theoretical data [26, 28]. For the other structures, to the best of our knowledge, no experimental or theoretical data are available for comparison. Thus, our results can serve as a prediction for future investigations. In all structures, there are no significant differences between their bulk moduli and between their equilibrium volumes which means,

at $T = 0$ K, that there may be no phase transitions occurring between these phases in the high pressure or occurring in the very high pressure. Moreover, the calculated total energy value for ST structure is about 0.1, 13, and 30 meV/atom lower in energy than for the WS, KS, and PMCA, respectively. Based on the energy consideration, the Cu_2MgSiS_4 can crystallise in the kesterite phase at room temperature (≈ 25 meV). Therefore, it is useful to investigate the mechanical stability, electronic and optical properties for this compound in the ST, WS, and KS phases.

3.2. Elastic properties

We calculated the elastic stiffness tensors of the Cu_2MgSiS_4 compound, in order to analyse its mechanical stability for the WS, ST and KS phases. Due to the symmetry $C_{ij} = C_{ji}$, the total number of independent components (elastic constants) can be reduced from 36 to 21 [36]. This number can be further reduced using the crystal symmetry to nine, for the orthorhombic crystal structure, seven for KS phase and only six for ST, the latter having tetragonal crystal structures. For the ST, which belongs to the tetragonal Laue group TI the expressions of the elastic moduli are well known, while for the KS belonging to the tetragonal Laue group TII, they have not been derived analytically yet. This is due to the fact that the off-diagonal shear elastic constant C_{16} is not necessarily equal to zero. However, with regard to the elastic properties, separation of the tetragonal solids into the two Laue groups is not strictly required: in each case, the elastic stiffness tensor may be described in terms of six parameters. Indeed, with a rotation around the z-axis through a given angle by [37, 38]:

$$\phi = (1/4)\tan^{-1}(4C_{16}/C_{11} - C_{12} - 2C_{66}), \quad (1)$$

which transforms the C_{ij} to C'_{ij} as given in Ref. [39], where C'_{16} is equal to zero, reducing the number of independent elastic constants from seven to six for the KS structure. Equation (1) gives two values for ϕ in the range $\phi < |\pi/2|$ that correspond to ϕ_1 and ϕ_2, where $\phi_1 = \phi_2 + \pi/4$ [38, 39]. In our case, we obtain $\phi_1 = -0.75°$, $\phi_2 = 44.24°$. The complete necessary and sufficient criteria of mechanical stability [40] for WS, ST, and KS phases respectively are

$$\begin{cases} C_{11} > 0; \quad C_{11}C_{22} > C_{12}^2 \\ C_{11}C_{22}C_{33} + 2C_{12}C_{13}C_{33} - C_{11}C_{23}^2 \\ \quad - C_{22}C_{13}^2 - C_{33}C_{12}^2 > 0 \\ C_{44} > 0; \quad C_{55} > 0; C_{66} > 0 \end{cases} \text{for WS,} \quad (2)$$

$$\begin{cases} C_{11} > |C_{12}|; \quad 2C_{13}^2 < C_{33}(C_{11} + C_{12}) \\ C_{44} > 0; \quad C_{66} > 0 \end{cases} \text{for ST,} \quad (3)$$

$$\begin{cases} C_{11} > |C_{12}|; \quad 2C_{13}^2 < C_{33}(C_{11} + C_{12}) \\ C_{44} > 0; \quad 2C_{16}^2 < C_{66}(C_{11} - C_{12}) \end{cases} \text{for KS.} \quad (4)$$

TABLE II

Calculated elastic constants (C_{ij}, GPa) and elastic parameters for Cu_2MgSiS_4 in four phases: bulk moduli (B_V, B_R, B_{VRH}, in GPa), shear moduli (G_V, G_R, G_{VRH}, in GPa), Pugh's indicator B/G, Young's moduli (E, in GPa), Poisson's ratio σ, Lame's constant (λ, in GPa), the elastic anisotropy indexes A^U.

C_{ij}	WS	ST	KT
C_{11}/C'_{11}	122.269	117.256	107.668 / 107.652[a], 129.509[b]
C_{22}	114.630		
C_{33}/C'_{33}	143.717	103.173	115.836 / 115.836[a,b]
C_{44}/C'_{44}	86.540	41.019	38.282 / 38.282[a,b]
C_{55}	33.569		
C_{66}/C'_{66}	36.833	41.555	41.689 / 41.704[a], 19.847[b]
C_{12}/C'_{12}	67.361	74.306	67.943 / 67.958[a], 46.101[b]
C_{13}/C'_{13}	58.947	70.945	71.610 / 71.610[a], 71.610[b]
C_{23}	53.451		
C_{16}/C'_{16}			0.5736 / 0[a,b]
B_V, B_R, B_{VRH}	82.237, 81.877, 82.057	85.564, 84.971,85.268	83.722, 83.464 ,83.593
A^U	0.9127	0.6623	0.5867
G_V, G_R, G_{VRH}	44.778, 37.894, 41.336	32.818, 29.015 ,30.916	31.651, 28.343, 29.997
E	106.179	82.748	80.376
λ	54.5	64.657	63.595
σ	0.284	0.338	0.34
B/G	1.985	2.758	2.787

[a]Rotation angle of $\phi_1 = -0.75°$; [b]Rotation angle of $\phi_2 = 44.24°$

The values of their independent elastic constants were estimated and are displayed in Table II, which are positive and satisfy the above stability criteria. $C_{11} > C_{33}$ in the ST phase implies that the bonding strength along the [100] and [010] direction is stronger than that of the bonding along the [001] direction, whereas the inverse trend is exhibited in WS and KS since $C_{11} < C_{33}$ for both phases. $C_{44} < C_{66}$ in the KS and ST phases, suggesting that the [100] (010) shear is more difficult than the [100] (001) shear, while the inverse behavior is showed by the WS phases since $C_{44} > C_{66}$. We have calculated the universal elastic anisotropy index for all phases as follows: $A^U = (5G_V/G_R + B_V/B_R - 6)$ [41], where we have found that the WS structure exhibits more elastic anisotropy among them. We notice that for the tetragonal ones the elastic anisotropies are approximately the same. In order to calculate the values of bulk moduli and shear moduli for polycrystalline materials, two main approximations are used: the Voigt and Reuss schemes [42]. The Voigt approximation is the upper limits of the above mentioned moduli, while the Reuss approximation corresponds to their lower limits. In addition, we have used the average of the Voigt and Reuss bulk and shear moduli, called the Voigt–Reuss–Hill (VRH) approximation [43], to calculate Young's modulus E, Lame's coefficient λ, and Poisson's ratio σ. The results are given in Table II.

Our calculation shows that Young's moduli of tetragonal structures are rather close to one another compared to the orthorhombic phase (see Table II), which show that they have the same stiffness, while the WS phase has more stiffness. Based on Pugh's [44] empirical relationship, the B/G ratio can classify materials as ductile or brittle according to a critical value. If $B/G > 1.75$ the material is ductile, otherwise the material is brittle. The values calculated for B/G for all phases indicate that the Cu_2MgSiS_4 compound is prone to ductile behavior.

3.3. Electronic properties

The calculated electronic band structures of Cu_2MgSiS_4 are shown in Fig. 3. The band structures of the three phases are quite similar. It can be seen that the WS, KS, and ST phases possess a direct band gap in the Γ–Γ direction of the Brillouin zone. The results are given in Table III. We find that the energy gap is increased from the ST to the WS, while the KS and ST phases have nearly the same gap. The corrected band gap according to the TB-mBJ calculation of WS is 2.442 eV, which is in agreement with the estimated experimental fundamental band gap about 2.6 eV from the onset of absorption spectrum Fig. 3a of Ref. [26]. For better comparison, the YS-PBE0 is also used to calculate the band gap of WS phase (more details are given in the section of optical properties).

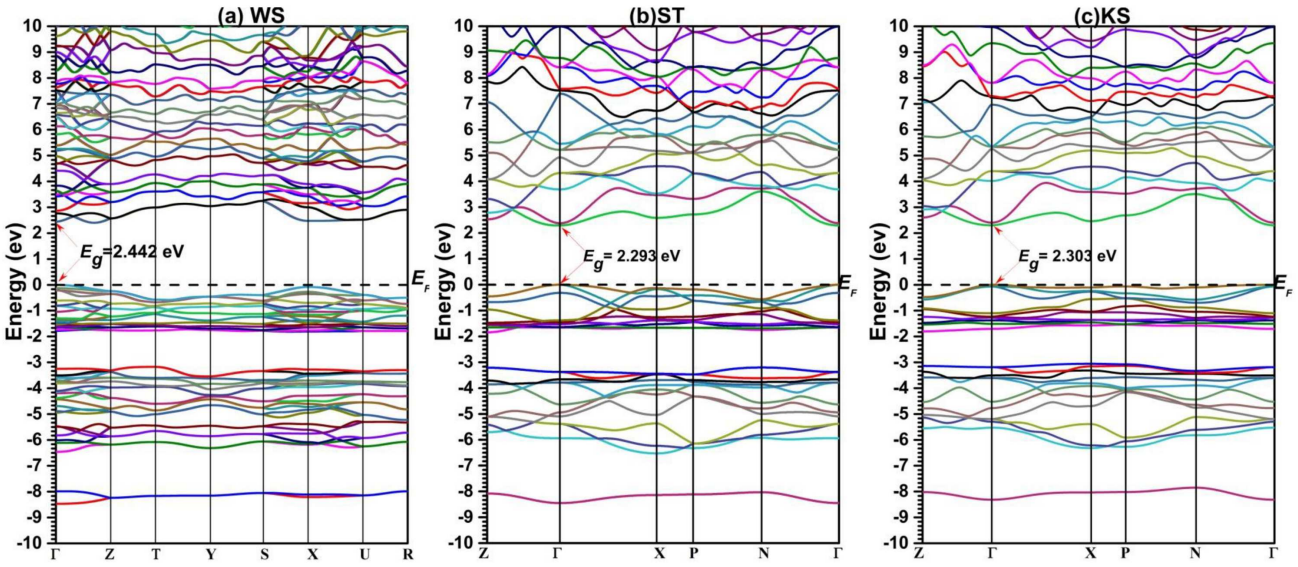

Fig. 3. Band structures along the principal high-symmetry directions in the Brillouin zone of Cu_2MgSiS_4 in (a) WS, (b) ST and (c) KS phases.

Since the band structures and the density of states (DOS) within the YS-PBE0 are almost similar to those reported by Ref. [26] they are not shown in this paper. The DOS has an important role in the analysis of physical properties of the materials. According to Fig. 4 of the total and partial DOS, we see that ST, KS, and even WS have the general features similar to each other. It is observed that the lower valence band in the energy range from –15.5 eV to –13.8 eV is mainly provided by the state S-*s*, and the upper valence band has three regions separated by gaps (labeled I, II, III), the first one from –8.61 to –7.82 is mainly provided by the S-*sp*, Si-*s* states, the second one from –6.65 to –3.00 is dominated by the Cu-*d*, Si-*p*, S-*p* states, the third one from –1.97 to 0 is

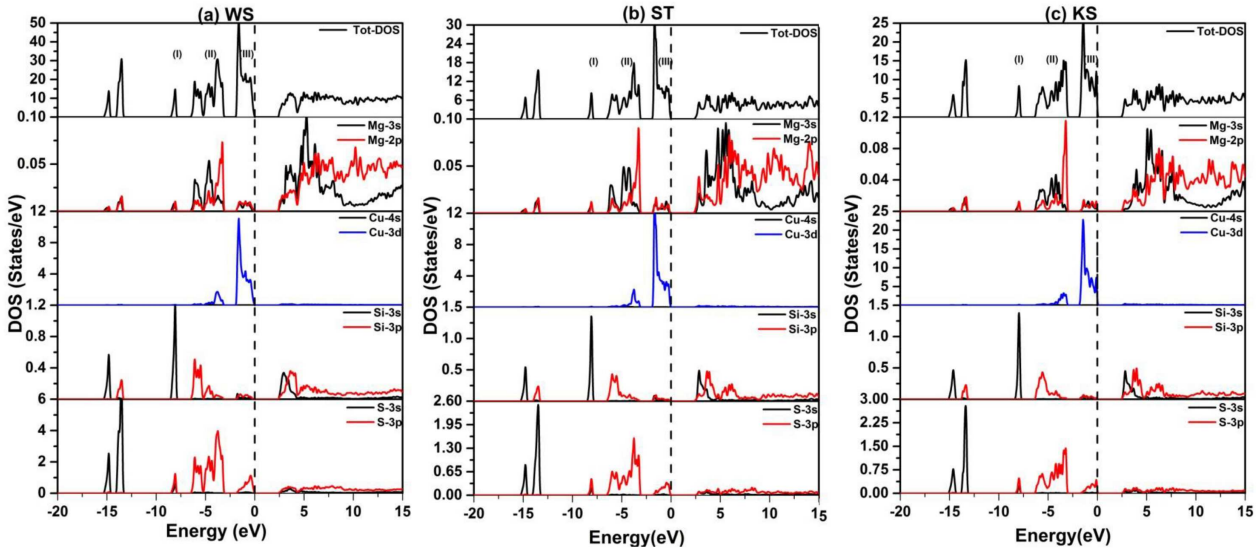

Fig. 4. Total and partial densities of states in (a) WS, (b) ST. and (c) KS phases.

strongly provided by Cu-*d*, less of S-*p* and little contribution of Si-*sp*. While the bottom conduction band above the Fermi level are almost dominated by the Si-*sp*, S-*p*, and Cu-*d* states with little contribution of Mg-*sp* states. The top valence band is mainly the antibonding component of the *p*–*d* hybridization between the anion S and the cation Cu. The bottom conduction band is mainly the antibonding component of the *s*–*s* and *s*–*p* hybridization between the cation Si and anion S with a significant contribution of Cu-*d* state. This band component is similar to that of Cu_2ZnSiS_4, where Zn does not contribute significantly to the band edge states [15].

3.4. Optical properties

The complex dielectric function is defined as the three-dimensional tensor $(\varepsilon^{\alpha\beta}(\omega) = \varepsilon_1^{\alpha\beta}(\omega) + \mathrm{i}\varepsilon_2^{\alpha\beta}(\omega)$, where $\alpha, \beta = x, y,$ or $z)$ that can be used to describe the linear response of the system to electromagnetic radiation, which relates to the interaction of the photons and electrons. The calculations ignore the excitonic and local field effects. There are two contributions to $\varepsilon^{\alpha\beta}(\omega)$, namely the intra-band and inter-band transitions. The contribution from intra-band transitions is important only for metals. The inter-band transitions can further be split into direct and indirect transitions. The indirect inter-band transitions which involved the scattering of phonons were ignored. The inter-band contribution to the imaginary part of the dielectric tensor components is calculated by summing transitions from occupied to unoccupied states over BZ, weighted with the appropriate momentum matrix elements as given by [45]:

$$\mathrm{Im}\varepsilon^{\alpha\beta}(\omega) = \frac{4\pi e^2}{m^2\omega^2}\sum_{i,f}\int \langle f|\, p_\alpha\, |i\rangle \langle i|\, p_\beta\, |f\rangle\, xW_i\,(1-W_f) \times\delta\,(E_f - E_i - \hbar\omega)\,\mathrm{d}^3k, \quad (5)$$

TABLE III

Band gaps of Cu_2MgSiS_4 in different phases.

Crystal structure	Fundamentals band gap [eV]	Optical band gap [eV]
WS	1.700*(GGA-PBEsol)	3.10*(TB-mBJ)
	2.442*(TB-mBJ)	3.20[a] (exp)
	3.204*(YS-PBE0)	3.80*(YS-PBE0)
	1.714[b](GGA-PBE)	
	2.01[a] (PP-PW)	
	3.208[b] (HSE06)	
ST	1.614*(GGA-PBEsol)	2.63*(TB-mBJ)
	2.293*(TB-mBJ)	
KS	1.726*(GGA-PBEsol)	2.58*(TB-mBJ)
	2.303*(TB-mBJ)	

[a]Ref. [26], [b]Ref. [28], *our work.

where e is the electron charge, m is the mass, $\langle f|\, p_\alpha\, |i\rangle$ and $\langle i|\, p_\beta\, |f\rangle$ are the dipole matrix elements corresponding to the α and β directions of the crystal (x, y or z), and f and i are the final and initial states, respectively. W_n is the Fermi distribution function for the n-th state and E_n is the electron energy in the n-th state. The dielectric function is a causal response function. Therefore, its real and imaginary parts are connected through the Kramers–Kronig relations. Furthermore, the other energy-dependent optical parameters, such as the reflectivity $R^{\alpha\beta}(\omega)$, energy-loss function $L^{\alpha\beta}(\omega)$, and absorption coefficient $\alpha^{\alpha\beta}(\omega)$ can be derived from $\varepsilon_1^{\alpha\beta}(\omega)$ to $\varepsilon_2^{\alpha\beta}(\omega)$ [45]. The respective crystal symmetries imply that there are two components of the optical parameters tensors for the tetragonal (ST and KS) structures and three for orthorhombic (WS) structure.

We calculate the real $\varepsilon_1^{\alpha\alpha}(\omega)$ and imaginary $\varepsilon_2^{\alpha\alpha}(\omega)$ parts of the dielectric tensor in each direction, as shown

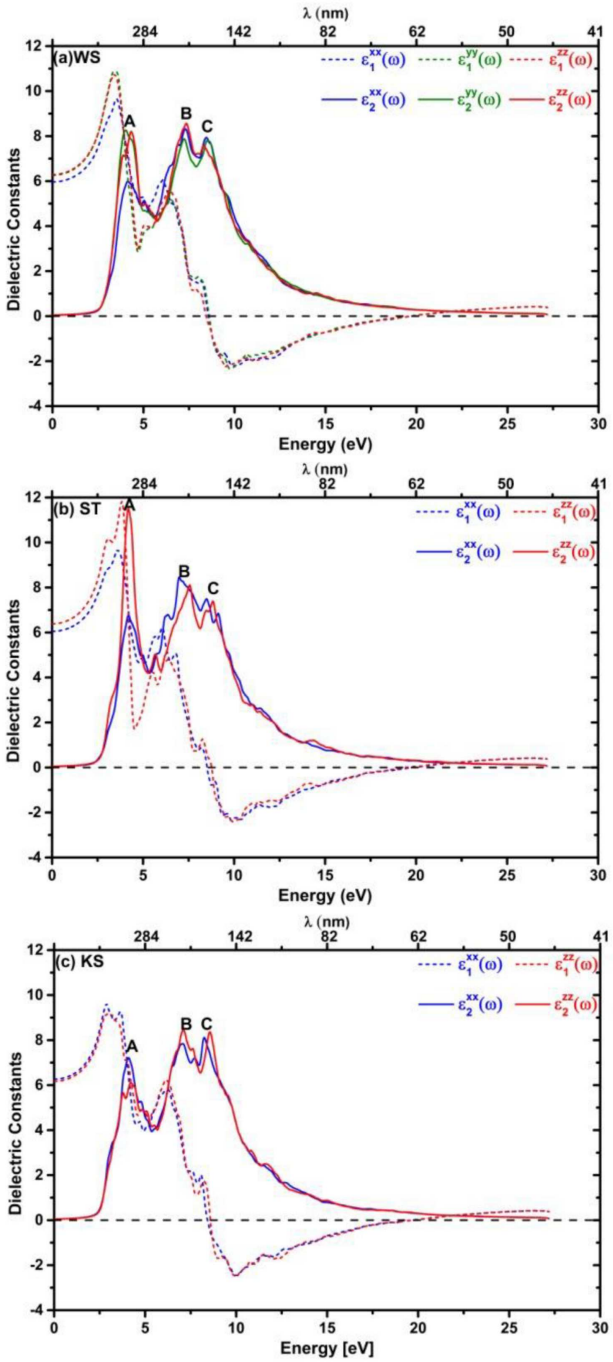

Fig. 5. The real and imaginary parts of the dielectric function for Cu_2MgSiS_4 in (a) WS, (b) ST, and (c) KS phases along crystallographic directions.

in Fig. 5. We can see that they exhibit the same shape for the three phases over a broad range of energy. This compound in its three phases does not exhibit a large optical anisotropy. However, the tetragonal phases show a little anisotropy between the two directions reflected by the behavior of the real parts $\varepsilon_1^{\alpha\alpha}(\omega)$ of their dielectric tensor as seen in Fig. 5b,c. For the orthorhombic phase, the two lattice constants b and c along the y and z directions, respectively, are almost equal; consequently, the dielectric tensor components along these directions are close to each other as if it were a tetragonal structure, while a relatively clear anisotropy is exhibited between the x and both these directions as seen in Fig. 5a.

The onsets of the calculated $\varepsilon_2(\omega)$ spectra corresponding to their first optical critical points occur at 2.44 eV for the three components of the WS phase, 2.29 and 2.30 eV for both components of the ST and KS phases, respectively, which correspond to the threshold of direct optical transition between the top of the valence band and the bottom of the conduction band at the Γ point for all phases, in good agreement with their respective fundamental band gaps. Beyond these points, the curves present several peaks. In particular, the $\varepsilon_2^{\alpha\alpha}(\omega)$ along each direction for all phases has three more pronounced peaks around 3.7–9 eV, labelled A, B, and C, which show an alternation of their heights with clear decrease going from ST to KS. The highest peaks positions are at around 7.34, 4.19, and 7.1 eV for the WS, ST and KS phases, respectively. The three successive highest peaks along each direction labelled A, B, and C in Fig. 5 originate from the electronic transitions from Cu-3d, S-3p in the upper valence band to the S-3p, S-3s, Si-3p, Si-3s states in the lower conduction band. Indeed, the peak A below 4.30 eV can be assigned to the transition from Cu-3d, S-3p in the third region (III) of the upper valence band to the S-3s, S-3p, Si-3s, Si-3p states in the lower conduction band, the peaks B, C in the range 5.34–9.80 eV can be attributed to the transition from Cu-3d, S-3p in the second region (II) of the upper valence band to the S-3p, Si-3p states in the conduction band. It is noted that the peak in $\varepsilon_2(\omega)$ does not correspond to a single interband transition since many transitions may be found in the band structure with an energy corresponding to the same peak [46]. For the real part spectrum, the main peaks (with magnitudes 9.65, 10.87, and 10.75 for $\varepsilon_1^{xx}(\omega)$, $\varepsilon_1^{yy}(\omega)$, and $\varepsilon_1^{zz}(\omega)$, respectively) for WS phase are situated around 3.38–3.51 eV; for the ST phase are located around 3.6–3.83 eV (9.66 and 11.82 for $\varepsilon_1^{xx}(\omega)$ and $\varepsilon_1^{zz}(\omega)$, respectively); for KS phase occur at 2.87 eV (9.62 and 9.17 for $\varepsilon_1^{xx}(\omega)$ and $\varepsilon_1^{zz}(\omega)$, respectively). We can see that the dielectric function for WS and ST phases display maximum anisotropy in the energy range 0–5.50 eV. The spectra curve of $\varepsilon_1^{\alpha\alpha}(\omega)$ crosses the zero line twice at ((8.55,19.66), (8.6,19.65), (8.44,19.69) for $\varepsilon_1^{xx}(\omega)$, $\varepsilon_1^{yy}(\omega)$, and $\varepsilon_1^{zz}(\omega)$, respectively), ((8.51,19.66) and (8.76,19.34)) for ($\varepsilon_1^{xx}(\omega)$ and $\varepsilon_1^{zz}(\omega)$, respectively) and ((8.42,19.68), (8.57,19.81) for $\varepsilon_1^{xx}(\omega)$ and $\varepsilon_1^{zz}(\omega)$, respectively)) for WS, ST, and KS, respectively. The $\varepsilon_1^{\alpha\alpha}(\omega) = 0$ is a necessary condition for plasma oscillations to occur but not a sufficient one [47]. Thus, the corresponding screened plasma frequencies [48] will be determined from the analysis of the electron energy-loss function. Furthermore, the static dielectric constants near zero-photon energy can be easily obtained as $\varepsilon_1^{xx}(\omega) = 5.96$, $\varepsilon_1^{yy}(\omega) = 6.26$, $\varepsilon_1^{zz}(\omega)(0) = 6.29$ for WS, $\varepsilon_1^{xx}(\omega) = 6.05$, $\varepsilon_1^{yy}(\omega) = 6.38$ for ST and $\varepsilon_1^{xx}(\omega) = 6.26$, $\varepsilon_1^{zz}(\omega) = 6.17$ for KS. For the

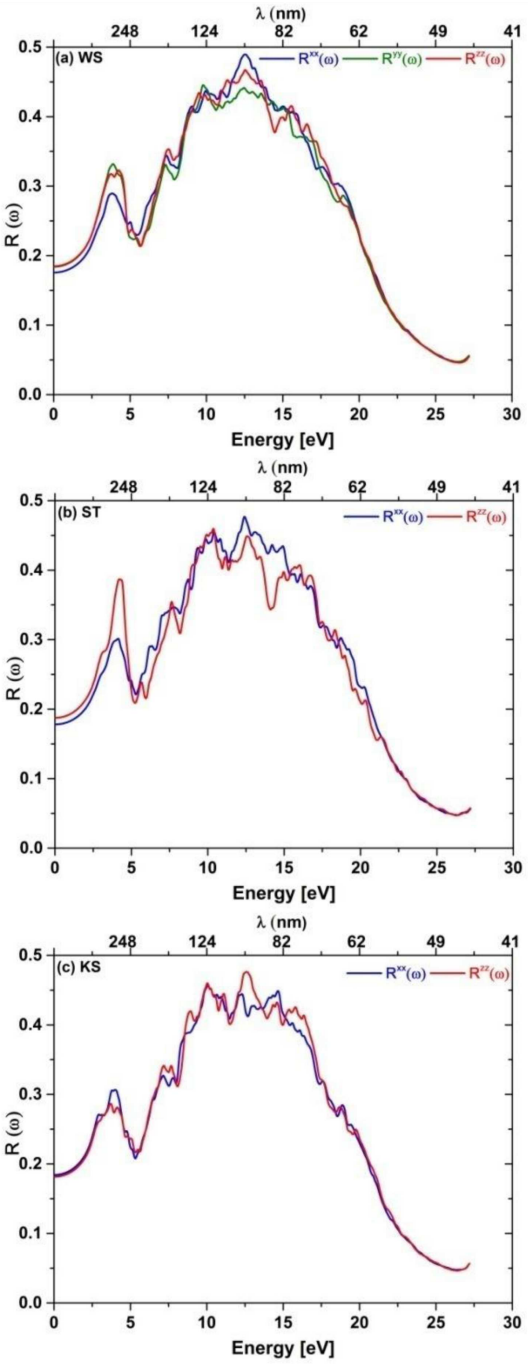

Fig. 6. Optical reflectivity for Cu_2MgSiS_4 in (a) WS, (b) ST, and (c) KS phases along crystallographic directions.

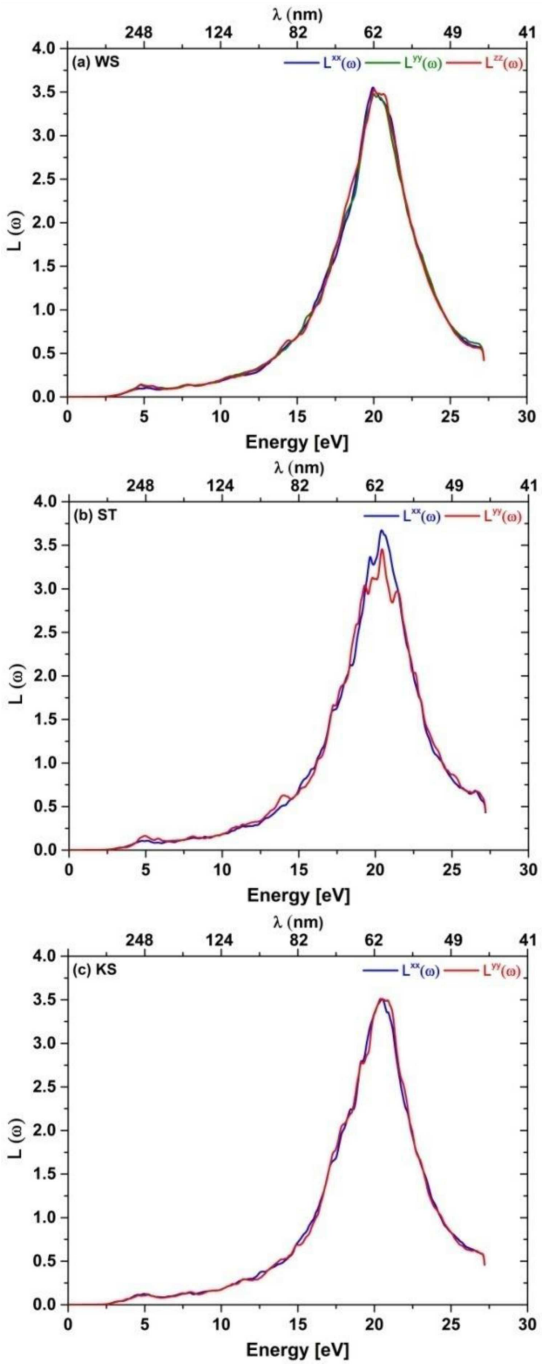

Fig. 7. Electron energy-loss spectrum for Cu_2MgSiS_4 in (a) WS, (b) ST, and (c) KS phases along crystallographic directions.

three phases, the directionally averaged values of zero frequency dielectric constants $\varepsilon_1(0)$ are near same for WS and ST with the values of 6.17, 6.16, respectively and slightly higher for the KS structure with the value of 6.23. On the other hand, in the absence of experimental data on the polarized zero frequency dielectric constant, no comment can be ascribed to the accuracy of our results.

The surface behavior of a material is characterized by its reflectivity $R(\omega)$, which is defined as the ratio of the incident power to the reflected power. Figure 6 displays the energy dependence of the different reflectivity components for the three phases up to 27 eV. We can see that they exhibit the same shape. Indeed, in the low energy range below 5 eV, isolated peaks occur and several peaks appear in the broad energy range 5–20 eV. The zero-frequency reflectivities are $R^{xx}(0) = 17.6\%$, $R^{yy}(0) = 18.4\%$, and $R^{zz}(0) = 18.5\%$ for WS, $R^{xx}(0) = 17.8\%$, $R^{zz}(0) = 18.7\%$ for ST, and $R^{xx}(0) = 18.4\%$,

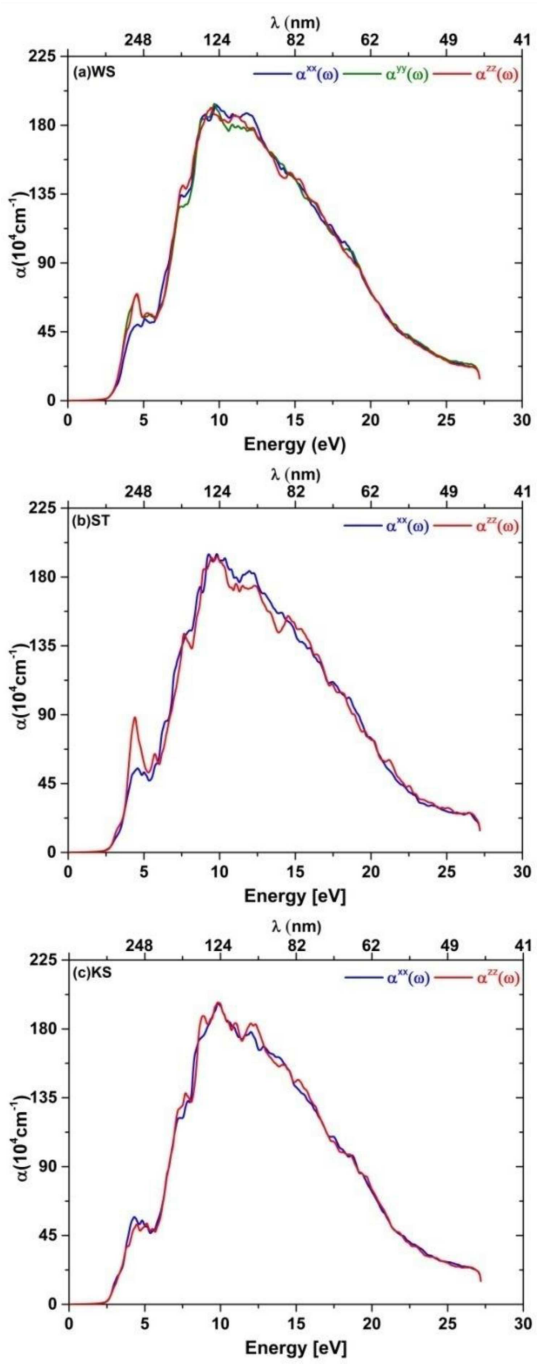

Fig. 8. Absorption coefficient for Cu_2MgSiS_4 in (a) WS, (b) ST, and (c) KS phases along crystallographic directions.

$R^{zz}(0) = 18.1\%$ for KS. The maximum reflectivity for WS (48.95%), ST (47.68%), and KS (47.63%) correspond to 12.55, 12.40, and 12.62 eV, respectively. It is worth underlining that the reflectivity along each direction $R^{\alpha\alpha}(\omega)$ reaches its maximum value when its corresponding $\varepsilon_1^{\alpha\alpha}(\omega)$ is below zero. For negative values of $\varepsilon_1(\omega)$, the materials are characterized as metals [49].

The electron energy-loss function describes the interaction by which energy is lost by a fast moving electron traveling the material. The sharp peaks of our calculated energy-loss function (Fig. 7) have maxima at 19.95, 20.41, and 20.49 eV for WS, ST, and KS, respectively, corresponding to their screened plasma frequencies above which the matter acts as a dielectric and below which it shows a metallic nature, in agreement with the second root of their respective $\varepsilon_1(\omega)$ ($\varepsilon_1(\omega) = 0$), and fits very well with the rapid decrease in reflectivity in Fig. 6.

The optical absorption coefficient $\alpha(\omega)$ is one of the most crucial evaluation criteria for the optical properties. Figure 8 displays the energy dependence of the absorption coefficient in each direction for the three phases up to 27 eV. Overall, they have similar absorption spectra. Indeed, they grow for photon energies higher than 2.44, 2.29, and 2.30 eV for WS, ST, and KS structures, respectively, which means that these phases start absorbing the radiation at wavelengths below 508, 540.5, and 538.1 nm, respectively. In addition, the region of intense absorption starts from these onsets to about 27 eV. The above mentioned energy regions consist of different spectral peaks occurring due to different electronic transitions where the highest peaks occur at 9.8, 9.81, and 9.84 eV for WS, ST, and KS structures, respectively, corresponding to an abrupt decrease of the $\varepsilon_2(\omega)$ shown in Fig. 8.

Since the available experimental band gap of this compound is determined optically by the UV-vis diffuse reflectance spectroscopy [26], and our calculation does not take into account the excitonic effects, the fundamental band gap is smaller than or equal to the optical band gap, depending on the possible transitions (selection rule) and the magnitude of dipole transition matrix elements. It should be reminded that the fundamental band gap is the energy difference between the highest occupied energy state of the valence band and the lowest unoccupied state of the conduction band, corresponding to the smallest energy which allows electrons to be thermally excited from the valence band to the conduction band. In contrast, the optical band gap is associated to the promotion of electrons from the valence band to the conduction band as a result of absorption of photons. Thus, we should take into account the difference between the two band gap concepts when comparing the theoretical results with the corresponding experimental data.

Unfortunately, the optical band gap is not reported in Ref. [28] using the screened hybrid HSE06 functional approach, then we have estimated it with the Yukawa-screened hybrid functional YS-PBE0 which is very similar to HSE06 for an appropriate value of the screening parameter λ [32]. Indeed, our value of fundamental band gap of WS phase using YS-PBE0 is in excellent agreement with that reported in Ref. [28] as shown in Table III.

In Fig. 9, only the directionally averaged optical absorption coefficient calculated with TB-mBJ for the three phases and YS-PBE0 approaches for the WS phase at the low energies up to 5 eV, are shown for a better comparison with experimental polycrystalline data. As expected, it can be seen in this figure that the different thresholds correspond to their respective calculated fundamental band

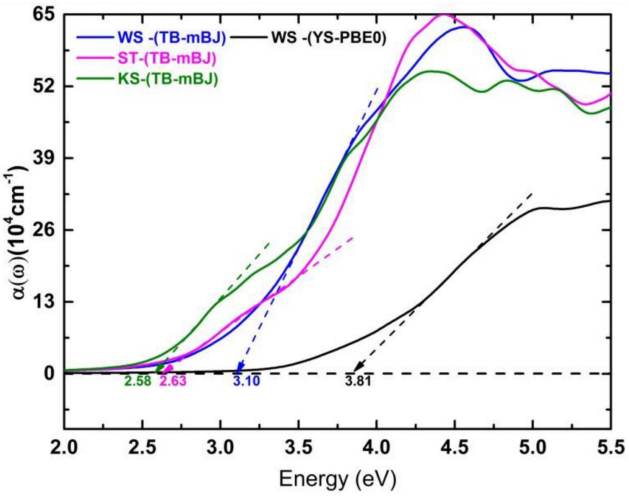

Fig. 9. Determination of optical band gap of Cu_2MgSiS_4 using TB-mBJ for WS, ST, and KS phases and YS-PBE0 for WS phase.

gaps (Table III). Therefore, for WS phase the experimental fundamental band gap can be estimated from Fig. 3a of Ref. [26] as about 2.6 eV which is in good agreement with TB-mBJ result compared to that of the YS-PBE0. We can expect that the YS-PBE0 and thus HSE06 overestimate optical band gap with respect to its experimental value. On the other hand, the optical band gaps are usually obtained through Tauc's plot method [50]. In this work, for more reliable comparison they are estimated by means of the same method used in Ref. [26]. Indeed, this is determined by the linear extrapolation of leading edges of the optical absorption coefficients, $\alpha(\omega)$, to the baseline, as shown in Fig. 9, and given in Table III. The TB-mBJ gives an optical band gap of the WS structure, in better agreement with experiment than those obtained with the YS-PBE0 which overestimates it with about 0.61 eV. Additionally, when comparing the TB-mBJ optical band gaps, we found that they decrease, going from the WS phase to the KS phase.

4. Conclusion

In present work, the structural, elastic, electronic, and optical properties of Cu_2MgSiS_4 have been investigated using the FP-LAPW+lo method within the GGA-PBEsol in the framework of the DFT. Our calculations for the Cu_2MgSiS_4 in different phases, namely WS, ST, KS, and PMCA show that the WS and ST phases are the most stable among them. The calculated structural parameters of the WS phase are in reasonable agreement with the available experimental and theoretical results. From our calculated elastic constants for the different phases this material is mechanically stable, could be classified as ductile material, and the WS structure exhibits the highest elastic anisotropy. On the other hand, following Pugh's empirical relationship, Cu_2MgSiS_4 behaves in a ductile manner for all phases. According to the TB-mBJ calculation, the Cu_2MgSiS_4 exhibits a semiconducting behavior with a direct band gap in the Γ–Γ direction for the others.

For the optical properties, it is found that the TB-mBJ calculation gives more reliable results than the other approaches. In particular, the estimated optical band gap of the WS phase is in good agreement with the experimental result. To our knowledge, there have not been any detailed theoretical results on the electronic and optical properties of Cu_2MgSiS_4 in ST and KS phases, including the dielectric function, the absorption coefficient, the reflectivity, and the energy-loss function. Therefore, we hope that our results could serve as a reference for future studies.

References

[1] G.M. Ford, Q. Guo, R. Agrawal, H.W. Hillhouse, *Chem. Mater.* **23**, 2626 (2011).

[2] X.Y. Shi, F.Q. Huang, M.L. Liu, L.D. Chen, *Appl. Phys. Lett.* **94**, 122103 (2009).

[3] G.H. McCabe, T. Fries, M.T. Liu, Y. Shapira, L.R. Ram-Mohan, R. Kershaw, A. Wold, C. Fau, M. Averou, E.J. McNiff, *Phys. Rev. B* **56**, 6673 (1997).

[4] E. Honig, H.S. Shen, G.Q. Yao, K. Doverspike, R. Kershaw, K. Dwight, A. Wold, *Mater. Res. Bull.* **23**, 307 (1988).

[5] Q. Guo, G.M. Ford, W.C. Yang, B.C. Walker, E.A. Stach, H.W. Hillhouse, R. Agrawal, *J. Am. Chem. Soc.* **132**, 17384 (2010).

[6] A. Goetzberger, C. Hebling, H.W. Schock, *Mater. Sci. Eng. R Rep.* **40**, 1 (2003).

[7] S. Medina, B. Bouhafs, P. Ruterana, *Computat. Mater. Sci.* **85**, 159 (2014).

[8] A. Ghosh, R. Thangavel, M. Rajagopalan, *En. Environm. Focus* **3**, 142 (2014).

[9] S. Levcenco, D. Dumcenco, Y.S. Huang, E. Arushanov, V. Tezlevan, K.K. Tiong, C.H. Du, *J. Alloys Comp.* **509**, 7105 (2011).

[10] Y. Li, W. Fan, H. Sun, X. Cheng, P. Li, X. Zhao, *J. Phys. Condens. Matter* **23**, 225401 (2011).

[11] M.L. Liu, I.W. Chen, F.Q. Huang, L.D. Chen, *Adv. Mater.* **21**, 3808 (2009).

[12] C. Sevik, T. Çağın, *Phys. Rev. B* **82**, 045202 (2010).

[13] T. Hirai, K. Kurata, Y. Takeda, *Solid-State Electron.* **10**, 9751 (1967).

[14] S. Chen, X.G. Gong, A. Walsh, S.H. Wei, *Phys. Rev. B* **79**, 165211 (2009).

[15] S. Chen, A. Walsh, Y. Luo, J.H. Yang, X.G. Gong, S.H. Wei, *Phys. Rev. B* **82**, 195203 (2010).

[16] L. Pauling, *J. Am. Chem. Soc.* **51**, 1010 (1929).

[17] P.A. Hersh, Ph.D. Thesis, Oregon State University, 2007.

[18] X. Li, J. Wang, Z. Zhao, S. Huang, W. Xie, *J. Appl. Phys.* **112**, 023701 (2012).

[19] C. Wang, S. Chen, J.H. Yang, L. Lang, H.J. Xiang, X.G. Gong, A. Walsh, S.H. Wei, *Chem. Mater.* **26**, 3411 (2014).

[20] D.B. Mitzi, O. Gunawan, T.K. Todorov, K. Wang, S. Guha, *Solar En. Mater. Solar Cells* **95**, 1421 (2011).

[21] S. Chen, X.G. Gong, C.G. Duan, Z.Q. Zhu, J.H. Chu, A. Walsh, Y.G. Yao, J. Ma, S.H. Wei, *Phys. Rev. B* **83**, 245202 (2011).

[22] Y. Zhang, X. Yuan, X. Sun, B.C. Shih, P. Zhang, W. Zhang, *Phys. Rev. B* **84**, 075127 (2011).

[23] V.A. Ocheretova, O.V. Parasyuk, A.O. Fedorchuk, O.Y. Khyzhun, *Mater. Chem. Phys.* **160**, 345 (2015).

[24] D. Chen, N.M. Ravindra, *J. Alloys Comp.* **579**, 468 (2013).

[25] M. Himmrich, H. Haeuseler, *Spectrochim. Acta Part A Mol. Spectrosc.* **47**, 933 (1991).

[26] B.W. Liu, M.J. Zhang, Z.Y. Zhao, H.Y. Zeng, F.K. Zheng, G.C. Guo, J.S. Huang, *J. Solid State Chem.* **204**, 251 (2013).

[27] K.E. Babu, A. Veeraiah, D.T. Swamy, V. Veeraiah, *Mater. Sci.-Poland* **30**, 359 (2012).

[28] D. Li, F. Ling, *Computat. Theor. Chem.* **1074**, 163 (2015).

[29] J.P. Perdew, A. Ruzsinszky, G.I. Csonka, O.A. Vydrov, G.E. Scuseria, L.A. Constantin, X. Zhou, K. Burke, *Phys. Rev. Lett.* **100**, 136406 (2008).

[30] F. Tran, P. Blaha, *Phys. Rev. Lett.* **102**, 226401 (2009).

[31] D. Koller, F. Tran, P. Blaha, *Phys. Rev. B* **85**, 155109 (2012).

[32] F. Tran, P. Blaha, *Phys. Rev. B* **83**, 235118 (2011).

[33] P. Blaha, K. Schwarz, G.K.H. Madsen, D. Kvasnicka, J. Luitz, *WIEN2 K, an Augmented Plane Wave + Local Orbitals Program for Calculating Crystal Properties*, Karlheinz Schwarz, Technische Universität, Wien 2001.

[34] F.D. Muranghan, *Proc. Natl. Acad. Sci. USA* **30**, 244 (1944).

[35] F. Birch, *Phys. Rev.* **71**, 809 (1947).

[36] J.F. Nye, *Physical Properties of Crystals: Their Representation by Tensors and Matrices*, Oxford University Press, 1985.

[37] P. Blanchfield, G.A. Saunders, *J. Phys C Solid State Phys.* **12**, 4673 (1979).

[38] J.M. Farley, G.A. Saunders, D.Y. Chung, *J. Phys. C Solid State Phys.* **6**, 2010 (1973).

[39] J.M. Farley, G.A. Saunders, *J. Phys. C Solid State Phys.* **5**, 3021 (1972).

[40] F. Mouhat, F.X. Coudert, *Phys. Rev. B* **90**, 224104 (2014).

[41] S.I. Ranganathan, M. Ostoja-Starzewski, *Phys. Rev. Lett.* **101**, 055504 (2008).

[42] W. Voigt, *Lehrbuch der Kristall-physik* (*Handbook of Crystal Physics*), 2nd ed., Teubner Press, Leipzig 1928.

[43] R. Hill, *Proc. Phys. Soc. Sect. A* **65**, 349 (1952).

[44] S.F. Pugh, *Lond. Edinb. Dublin Philos. Mag. J. Sci.* **45**, 823 (1954).

[45] C. Ambrosch-Draxl, J.O. Sofo, *Comput. Phys. Commun.* **175**, 1 (2006).

[46] S. Cabuk, *Philos. Mag.* **96**, 190 (2016).

[47] T.B. Nasr, H. Maghraoui-Meherzi, H.B. Abdallah, R. Bennaceur, *Physica B Condens. Matter.* **406**, 287 (2011).

[48] F. Wooten, *Optical Properties of Solids*, University of California, New York 1972.

[49] B. Xu, X. Li, J. Sun, L. Yi, *Europ. Phys. J. B* **66**, 483 (2008).

[50] F. Yakuphanoglu, *Solar En.* **85**, 2518 (2011).